Journal of Computational Physics **172,** 326–347 (2001)
doi:10.1006/jcph.2001.6826, available online at http://www.idealibrary.com on IDEAL®

Self-consistent Numerical Simulation of Isotope Separation by Selective Ion Cyclotron Resonance Heating in a Magnetically Confined Plasma

P. Omnes and P. Louvet

Commissariat à l'Energie Atomique, Centre d'Etudes de Saclay, Direction du Cycle du Combustible, Département des Procédés d'Enrichissement, 91191 Gif sur Yvette Cedex, France
E-mail: pomnes@cea.fr

Received October 31, 2000; revised May 9, 2001

A self-consistent nonlinear model of an isotope separation process based on selective ion cyclotron resonance heating in a magnetized plasma is presented, and its numerical resolution is described. The response of the electrons to the electromagnetic field is modeled by a cold and linear conductivity tensor, while a particle method is used to solve nonlinear Vlasov equations for the ions. The resolution of the time-harmonic Maxwell equations is achieved by a finite-element method. Both steps are coupled by an iterative procedure, which shows fast convergence. Results are presented for the case of a solenoidal launching antenna.

Key Words: Ion cyclotron resonance heating; isotope separation; Vlasov–Maxwell equations; finite element method; particle method.

1. INTRODUCTION

The ion cyclotron resonance (ICR) phenomena allows to give energy to species in a magnetized plasma. Such effects have been commonly used for a long time, for example in fusion devices [1] as well as in isotope separation [2, 3]. In this last case, one chosen species has to be heated selectively by the electric field created by an inductive antenna. A schematic description of a device used for isotope separation is given by Fig. 1. A strongly magnetized plasma is first created in the source zone by collisions of the atoms of a metallic vapor and electrons heated at the electron cyclotron frequency. Ions and electrons leave the source and enter the zone we want to modelize in this paper, where ions are heated selectively by cyclotron resonance. Then, sufficiently heated ions, which have large Larmor radii, hit the enriched plates in the collection zone, while nonresonating ions hit the terminal waste plate. The efficiency of this process requires that ion–ion collisions are rare, so that selective

0021-9991/01 $35.00

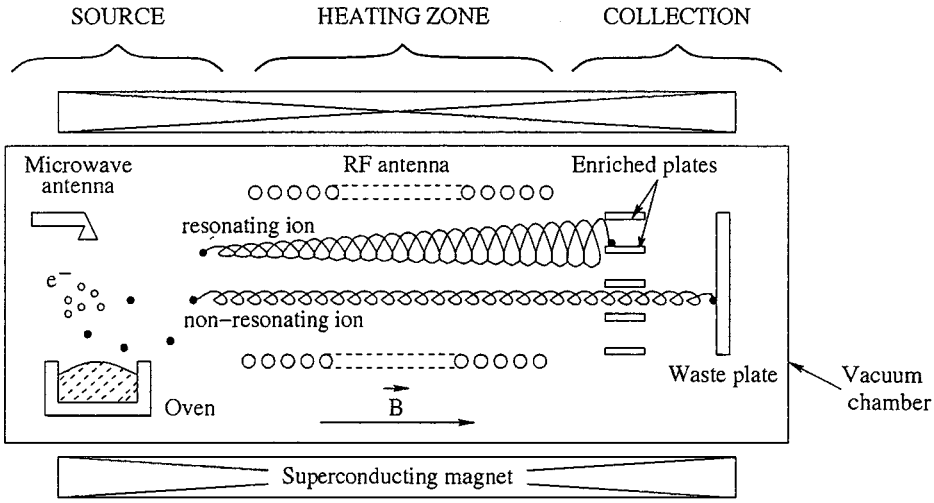

FIG. 1. Schematic view of an isotope separation device.

heating is not spoiled by collisional transfer of energy between resonant and nonresonant species. Therefore, collisions are usually neglected in the modelization. More complete descriptions of such devices can be found in [2, 3].

The simulation of ICR heating remains a difficult problem as the nonlinear Maxwell–Vlasov system of equations has to be solved for this magnetized noncollisional plasma. As the unsteady phase is usually of reduced interest for isotope separation devices, time-periodic solutions of these equations are generally considered.

Following the ideas of McVey [4], a semi-analytical derivation was developed by Compant La Fontaine and Pashkovsky [5]. They resolved the Maxwell equations in the time-harmonic representation and in cylindrical coordinates (r, θ, z), where z is the axis of the confining magnetic field. The solutions for the electromagnetic (EM) field $(\mathbf{E}, \mathbf{B})$ are found in terms of Fourier series, both in the azimuthal mode n and in the axial wavenumber $k_\parallel$. The current density generated by the plasma species is set equal to $\sigma(\omega, n, k_\parallel)\, \mathbf{E}(\omega, n, k_\parallel)$, where ω is the frequency of the exciting current density carried by the launching antenna, and where σ is a conductivity tensor obtained by the integration over velocities of the solutions of the Laplace–Fourier transformed Vlasov equations, linearized around spatially infinite and homogeneous time-averaged zeroth-order distribution functions. Its expression, calculated for a homogeneous magnetic field $\mathbf{B}_0$ is given for example by Ginzburg and Ruhadze [6]. Moreover, a greatly simplified formulation of this tensor is used in [5] by setting $k_\perp \rho_L \ll 1$, where $k_\perp$ is the transverse wavenumber and ρ_L the mean transverse Larmor radius of the species.

This method has the major defect of being linear in the field amplitude, neglecting the quasilinear retroaction of the wave on the ion zeroth-order distribution functions. It is also inconsistent with the plasma flow: In actual experiments, the temperature of the heated species may vary from around 5 eV at the entrance to about 500 eV at the end of the device, which contradicts the assumed axial homogeneity. Thus, it can be applied mainly to heating in the linear range, mostly for minor species. Moreover, finite axial length effects are ignored, though it can be shown [7, 8] that this may have consequences on the Landau and cyclotron damping rates as compared to those of an infinite plasma. Furthermore, this

method needs a Fourier transform of the exciting current density, which often leads to quite tedious computations as usually the antenna shape is complicated (helicoidal filaments with terminal rings and current leads). Details about this method, as well as comparisons with the experiments can be found in [4, 5, 9].

Because of these restrictive hypotheses, it was decided to develop a self-consistent numerical solution of the Maxwell–Vlasov system in configuration space rather than in the Fourier space, assuming that a time-periodic regime has been reached. A quasilinear model is derived, which retains only the coupling introduced by the harmonics -1, 0, and 1 of the fields and of the ion distribution functions, while the contribution of the electrons is assumed to be cold and linear. Moreover, neutrality of the time-averaged quantities is assumed.

In order to solve the coupled system of equations, we developed an iterative fixed-point method. In the first step, the Maxwell equations are solved in time-harmonic form by a finite element method with sources computed at the previous iteration. Then, the Vlasov equations for the ions are solved by a particle method with the newly computed EM wave field. The procedure is iterated until a fixed point is reached. Fast convergence is obtained by approximately impliciting the ionic current with the help of an equivalent, linear, and local conductivity tensor.

This paper is organized as follows. In Section 2, we first derive and justify the physical model we use, and give the corresponding governing equations. Then, in Section 3, the iterative method employed to find a solution of the model is detailed, and the underlying numerical methods are described. In Section 4, we present and discuss results obtained by our method, including resonance curves, field, and mean Larmor radius radial and longitudinal profiles for a solenoidal launching antenna. In Section 5, conclusions are drawn and the results are summarized.

2. MODELIZATION

2.1. *General Assumptions*

As mentioned earlier, we intend to solve the Maxwell–Vlasov system

$$\frac{\partial f_\alpha}{\partial t} + \mathbf{V}\cdot\nabla_{\mathbf{X}} f_\alpha + \frac{q_\alpha}{m_\alpha}(\mathbf{E}+\mathbf{V}\times\mathbf{B})\cdot\nabla_{\mathbf{V}} f_\alpha = 0, \tag{1}$$

$$\mathbf{J}(\mathbf{X},t) = \sum_{\alpha\in\varepsilon} q_\alpha \int_{\mathbb{R}^3} f_\alpha(\mathbf{X},\mathbf{V},t)\mathbf{V}d^3\mathbf{V}, \tag{2}$$

$$\frac{1}{c^2}\frac{\partial \mathbf{E}}{\partial t} - \nabla\times\mathbf{B} = -\mu_0(\mathbf{J}+\mathbf{J}_{ext}), \tag{3}$$

$$\frac{\partial \mathbf{B}}{\partial t} + \nabla\times\mathbf{E} = 0 \tag{4}$$

in a time-periodic representation and inside a bounded domain which represents the heating region. This domain is supposed to be a cylinder whose end sections are located in $z = 0$ and $z = L$. The confining magnetic field is directed along the z axis, and we shall denote by (e_x, e_y, e_z) the orthonormal basis of $\mathbb{R}^3$.

In these equations, the subscript α refers to any element (electrons or ions) in the set ε of the plasma species, and q_α, m_α, and f_α are the charge, mass, and particle distribution function, respectively, of the species α whose cyclotron frequency is given by $\omega_{c\alpha} = \frac{q_\alpha|\mathbf{B}_0|}{m_\alpha}$.

Because the current $\mathbf{J}_{ext}$ carried by the inductive antenna is purely harmonic,

$$\mathbf{J}_{ext}(t) = \mathbf{J}_{ext,1}e^{i\omega t} + \bar{\mathbf{J}}_{ext,1}e^{-i\omega t}, \tag{5}$$

the solution is searched under the form

$$A(t) = A_0 + A_1 e^{i\omega t} + \bar{A}_1 e^{-i\omega t}, \tag{6}$$

where A denotes either $\mathbf{E}$, $\mathbf{B}$ or f_α. This means that only the harmonics -1, 0, and 1 (i.e., the time-independent solution and the fundamental harmonics) are taken into account. Indeed, in ICR isotope separation experiments, the EM force created by the fields $\mathbf{E}_1$, $\mathbf{B}_1$ acting on the particles is small as compared to that created by the stationary field $\mathbf{B}_0$. In other words, $|\mathbf{B}_1| \sim \lambda|\mathbf{B}_0|$ and $|\mathbf{E}_1| \sim \lambda|\mathbf{V}_c||\mathbf{B}_0|$, where λ is much smaller than 1, and where $\mathbf{V}_c$ is a characteristic velocity of the plasma species, the thermal velocity for example. When developing the solution of the Vlasov equation (1) in ascending powers of λ, it can be shown that the total contribution of higher-order terms $f_{\alpha,p}$ with $|p| \geq 2$ of the distribution function f_α is of order λ^2. Consequently, because of the linearity of Eqs. (3) and (4), $\mathbf{E}_p$ and $\mathbf{B}_p$ with $|p| \geq 2$ are also of order up to λ^2. This fact is well confirmed by the experimental results, as no higher harmonics are observed.

Further, the static electric field is assumed negligible ($\mathbf{E}_0 \approx 0$), because of the great axial mobility of electrons: When positive charges are in excess in a section of the plasma, because of ICR heating or of other plasma phenomena, then the electrons located on the same magnetic field lines, but in other sections of the plasma, are able to neutralize quite easily this space-charge [4]. This assumption is used in most of the works relative to ICR isotope separation [4, 5] and is also fairly well-checked in practice. Moreover, we shall consider that the highly confined plasma is low β, so that the value of the externally applied magnetic field $\mathbf{B}_0$ is considered to be known and is not disturbed by the time-averaged current densities generated by the particles. Although the method presented here does not need any restriction on the homogeneity of the static magnetic field, we will assume it homogeneous throughout the whole heating region for the sake of simplicity.

2.2. *Modelization of the Electrons*

The response of the electrons under the action of the EM field is assumed linear because the typical transit time of an electron crossing the heating zone with thermal velocity is of the order of some microseconds, so that the interaction time with the wave is a very few periods (compared to 500 to 1000 for the ions). Moreover, electron cyclotron absorption is negligible as $\omega \ll \omega_{ce}$. Electron Landau damping has also been neglected as the z component of $\mathbf{E}_1$ is usually very weak because of the high electronic axial conductivity. Finally, the mean electron Larmor radius ($\rho_{Le} \sim 5\ \mu$m) is much smaller than the gradient scale length of the EM field ($k_\perp \rho_{Le} \ll 1$), and the phase velocity of the wave is usually large in front of the electron mean axial velocity $\bar{w}_e$ ($\bar{w}_e \ll \frac{\omega}{k_\parallel}$).

With these assumptions, we end up with a cold electron conductivity tensor relating the first harmonic of the electronic current density $\mathbf{J}_{e,1}$ and $\mathbf{E}_1$ in the following way [10]

$$\mathbf{J}_{e,1} = n_{e,0}\chi_e \mathbf{E}_1, \tag{7}$$

where $n_{e,0}$ is the time-averaged electronic density, and χ_e is given by

$$\chi_e = \frac{q^2}{m_e}\begin{pmatrix} -ia_e & b_e & 0 \\ -b_e & -ia_e & 0 \\ 0 & 0 & -ir_e \end{pmatrix}, \tag{8}$$

with the definitions

$$a_e = \frac{1}{2}(s_e + d_e), \quad b_e = \frac{1}{2}(s_e - d_e), \tag{9}$$

$$s_e = \frac{1}{\omega + \omega_{ce}}, \quad d_e = \frac{1}{\omega - \omega_{ce}}, \quad r_e = \frac{1}{\omega}. \tag{10}$$

Consistently with the hypothesis made in Section 2.1 on the nullity of the static electric field, the plasma is assumed neutral so that

$$n_{e,0} = \sum_{i \in \mathcal{I}} n_{i,0}, \tag{11}$$

where $\mathcal{I}$ denotes the set of the isotopic ion species and $n_{i,0}$ the time-averaged density of the ion species $i \in \mathcal{I}$.

2.3. *Modelization of the Ions*

As the efficiency of the isotope separation device under consideration relies mainly on the dynamics of the different ion species, we retain the full Vlasov equation (1) for these species, where the fields **E** and **B** are now under the form (6). The only restriction we make is that the solution of (1) is supposed to be time-periodic. The existence of such a solution was proved by Bostan and Poupaud [11] and by Omnes [12]. Note that, on the other hand, the existence of a periodic solution to the whole Vlasov–Maxwell system in a three-dimensional bounded domain has not been proved yet. We shall also suppose that the incoming ion distribution functions are known and time-independent on the injection boundary located in $z = 0$ and that no particle is reflected from the end boundary of the device located in $z = L$

$$f_\alpha(\mathbf{X}, \mathbf{V}, t) = f_{\alpha,B}(\mathbf{X}, \mathbf{V}) \quad \text{for } z = 0 \text{ and } V_z > 0, \tag{12}$$

$$f_\alpha(\mathbf{X}, \mathbf{V}, t) = 0 \quad \text{for } z = L \text{ and } V_z < 0, \tag{13}$$

where $f_{\alpha,B}(\mathbf{X}, \mathbf{V})$ is a given, not necessarily Maxwellian, distribution function. In particular, the **X**-dependence of $f_{\alpha,B}$ allows to model radially nonhomogeneous plasmas.

2.4. *Summary of the Model*

Using the previous considerations, the full system to be solved is: For given $\mathbf{J}_{ext,1}$ and distribution functions $f_{\alpha,B}$ of the ions on the boundaries, find f_α, $\frac{2\pi}{\omega}$ periodic with $\alpha \in \mathcal{I}$ and $\mathbf{E}_1$, $\mathbf{B}_1$ such that

$$\frac{\partial f_\alpha}{\partial t} + \mathbf{V} \cdot \nabla_{\mathbf{X}} f_\alpha + \frac{q_\alpha}{m_\alpha}[(\mathbf{E}_1 e^{i\omega t} + \overline{\mathbf{E}_1} e^{-i\omega t} + \mathbf{V} \times (\mathbf{B}_0 + \mathbf{B}_1 e^{i\omega t} + \overline{\mathbf{B}_1} e^{-i\omega t})] \cdot \nabla_{\mathbf{V}} f_\alpha = 0, \tag{14}$$

$$\nabla \times \nabla \times \mathbf{E}_1 - \left(\frac{\omega^2}{c^2} I_3 - \mu_0 i\omega n_{e,0} \chi_e \right) \mathbf{E}_1 = -\mu_0 i\omega (\mathbf{J}_{ext,1} + \mathbf{J}_{i,1}), \tag{15}$$

$$i\omega \mathbf{B}_1 = -\nabla \times \mathbf{E}_1, \tag{16}$$

where I_3 is the identity matrix of $(\mathbb{R}^3)^2$, $\mathbf{J}_{i,1}$ is the fundamental harmonic of the ion current density,

$$\mathbf{J}_{i,1} = \sum_{\alpha \in \mathcal{I}} q_\alpha \int_{\mathbb{R}^3} \mathbf{V}\, d^3\mathbf{V} \frac{\omega}{2\pi} \int_0^{\frac{2\pi}{\omega}} e^{-i\omega t} f_\alpha(t)\, dt, \tag{17}$$

and where, according to Eq. (11), $n_{e,0}$ is set equal to

$$n_{e,0} = \sum_{\alpha \in \mathcal{I}} \int_{\mathbb{R}^3} d^3\mathbf{V} \frac{\omega}{2\pi} \int_0^{\frac{2\pi}{\omega}} f_\alpha(t)\, dt. \tag{18}$$

Boundary conditions for the EM fields will be discussed later on.

Note that we have combined Eqs. (3) and (4) to get Eq. (15), which is more convenient for the numerical approximation considered in Section 3.2. Moreover, Eq. (14) allows for a quasilinear description of the behavior of the ions, which self-consistently models the heating of these species

$$i\omega f_{\alpha,1} + \mathbf{V} \cdot \nabla_{\mathbf{X}} f_{\alpha,1} + \frac{q_\alpha}{m_\alpha} (\mathbf{V} \times \mathbf{B}_0) \cdot \nabla_{\mathbf{V}} f_{\alpha,1} = -\frac{q_\alpha}{m_\alpha} (\mathbf{E}_1 + \mathbf{V} \times \mathbf{B}_1) \cdot \nabla_{\mathbf{V}} f_{\alpha,0}, \tag{19}$$

$$\mathbf{V} \cdot \nabla_{\mathbf{X}} f_{\alpha,0} + \frac{q_\alpha}{m_\alpha} (\mathbf{V} \times \mathbf{B}_0) \cdot \nabla_{\mathbf{V}} f_{\alpha,0} = -2 \frac{q_\alpha}{m_\alpha} \Re e\, [(\mathbf{E}_1 + \mathbf{V} \times \mathbf{B}_1) \cdot \nabla_{\mathbf{V}} \bar{f}_{\alpha,1}]. \tag{20}$$

3. NUMERICAL SOLUTION OF THE MODEL

As is well-known in plasma physics, the dielectric conductivity tensor (i.e., the relation linking $\mathbf{J}_{i,1}$, given by Eq. (17), to the field $\mathbf{E}_1$) is essentially nonlocal, and the discretization of a wave equation with such a tensor would then lead to a full mass-matrix, which is prohibitive both in computational time and memory storage requirements. This is the reason why, as outlined by Van Eester [13], the numerical methods usually developed until now consider mainly nonlocality in only one space dimension, normally to the static magnetic field $\mathbf{B}_0$. The idea proposed in the present article is to compute an "equivalent" conductivity tensor (to be defined in the next subsection), linear and local, and to use a fixed-point iterative method to get the solution of system (14) to (18).

3.1. *Description of the Numerical Method*

We first describe the iterative method used to compute a solution of the proposed model. Knowing the values of the fields and of the distribution functions $\mathbf{E}_1^k$, $\mathbf{B}_1^k$ and f_α^k with $\alpha \in \mathcal{I}$ after the k^{th} iteration, the steps for the $(k+1)^{\text{th}}$ iteration are the following

- First, compute $\mathbf{J}_{i,1}^k(\mathbf{X})$ and $n_{e,0}^k(\mathbf{X})$ respectively by formula (17) and (18).
- In each point of the domain, compute an "equivalent," linear and local ionic conductivity tensor $\sigma_i^{k+1}(\mathbf{X})$, using $\mathbf{J}_{i,1}^k(\mathbf{X})$ and $\mathbf{E}_1^k(\mathbf{X})$ according to the relation

$$\mathbf{J}_{i,1}^k(\mathbf{X}) = \sigma_i^{k+1}(\mathbf{X})\, \mathbf{E}_1^k(\mathbf{X}). \tag{21}$$

Here, we must point out that there is a large choice of such tensors, because there are nine coefficients in the 3×3 matrix $\sigma_i^{k+1}(\mathbf{X})$ and only three equations in formula (21). The fact that the σ_{xz}, σ_{yz}, σ_{zx}, and σ_{zy} elements of the conductivity tensor are dominated by the remaining coefficients when the plasma is not too hot, leads us to choose the particular form

$$\sigma_i^{k+1} = \begin{pmatrix} -ia^{k+1} & b^{k+1} & 0 \\ -b^{k+1} & -ia^{k+1} & 0 \\ 0 & 0 & -ir^{k+1} \end{pmatrix}, \tag{22}$$

where the three unknowns a^{k+1}, b^{k+1}, and r^{k+1} are now fully determined by formula (21).

- Calculate the electronic conductivity tensor

$$\sigma_e^{k+1}(\mathbf{X}) = n_{e,0}^k(\mathbf{X})\chi_e. \tag{23}$$

- Solve the wave equation with the new tensors

$$\nabla \times \nabla \times \mathbf{E}_1^{k+1} - \left(\frac{\omega^2}{c^2} I_3 - \mu_0 i\omega \left(\sigma_e^{k+1} + \sigma_i^{k+1} \right) \right) \mathbf{E}_1^{k+1} = -\mu_0 i\omega \mathbf{J}_{ext}, \tag{24}$$

At this level, it must be noticed that $\sigma_i^{k+1}\mathbf{E}_1^{k+1}$ represents an implicit prediction of $\mathbf{J}_{1,i}^{k+1}$ and σ_e^{k+1} a prediction of the converged value of $n_{e,0}(\mathbf{X})\chi_e$.

- Solve Eq. (16) for $\mathbf{B}_1^{k+1}$.
- Solve Eq. (14) for f_α^{k+1} with the newly computed fields $(\mathbf{E}_1^{k+1}, \mathbf{B}_1^{k+1})$.

If this procedure converges to a limit, then it is easy to check that this limit is a solution of the initial system (14) to (18). Moreover, if there is a unique solution to this system (which remains an open question), then the choice of the form of σ_i in Eq. (21) does not influence the final result, but only the speed of convergence. If this tensor is badly chosen, there might even be no convergence at all. Although no theoretical tool has been developed to optimize the choice of such a tensor and to study under which conditions this procedure converges, it seems very natural to use a tensor that is as close as possible to the "true" physical relation linking $\mathbf{J}_{i,1}$ to the field $\mathbf{E}_1$. For the kind of devices we are concerned with, in which the plasma is not very hot (see the parameters given in Section 4.1), an efficient choice for achieving convergence is thus given by the particular form Eq. (22), as can be seen from the convergence criteria defined by Eqs. (88) and (89) and plotted on Figs. 2 and 3.

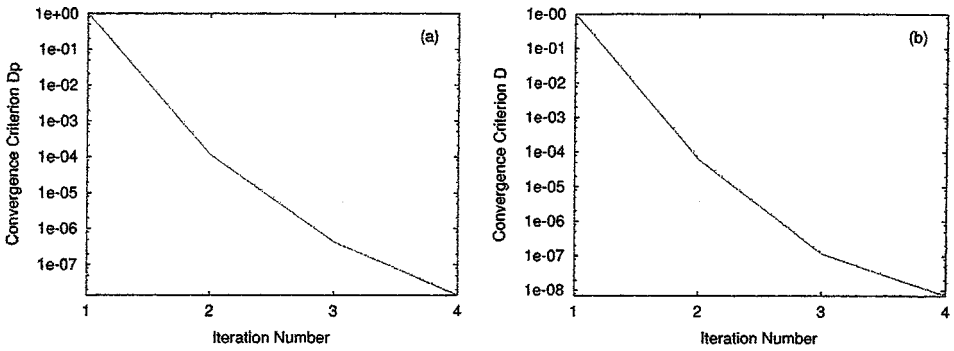

FIG. 2. Value of the convergence criteria Dp^k (a) and D^k (b) as a function of the iteration number k for $\omega = 0.95\omega_{c1}$.

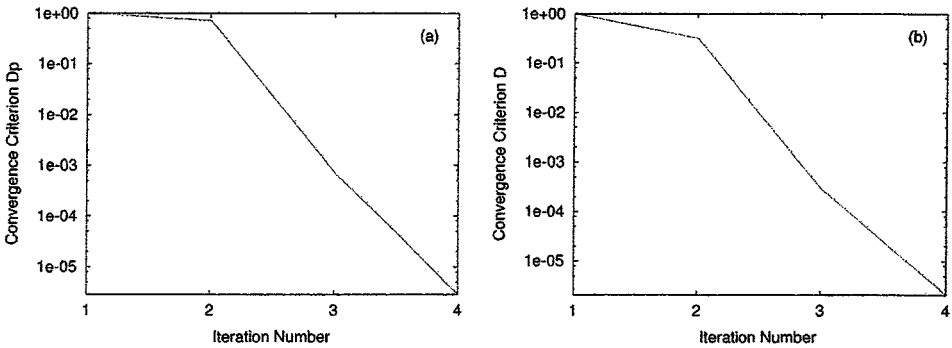

FIG. 3. Value of the convergence criteria Dp^k (a) and D^k (b) as a function of the iteration number k for $\omega = \omega_{c1}$.

The proposed numerical method relies on two main steps: The resolution of the wave equation (24) with given conductivity tensors, and the resolution of the Vlasov equation (14) with given fields. These two points are the items of the next two subsections.

3.2. *Solution of the Maxwell Equations*

The resolution of the first step of the iterative method, i.e., the solution of the Maxwell harmonic equation (24), is performed by a finite element method using P^1 tetrahedral elements. They were chosen rather than edge elements [14] because the particle pushing method described in Section 3.3 requires the continuity of the EM fields. For a complete review of the respective advantages of both finite element methods, we refer to [15]. Numerical experiments show that P^1 elements are appropriate in our case, as there is no singularity in the geometry of the computational domain and no discontinuity in the dielectric tensor coefficients.

3.2.1. Variational Formulation. In the continuous case, Gauss' law

$$\nabla \cdot (\varepsilon \mathbf{E}_1) = i\omega\mu_0 \nabla \cdot \mathbf{J}_{ext,1} \quad \text{with } \varepsilon = \frac{\omega^2}{c^2} I_3 - \mu_0 i\omega\left(\sigma_e^{k+1} + \sigma_i^{k+1}\right) \tag{25}$$

is a direct consequence of Eq. (24), but it has been shown by Jiang *et al*. [16] that neglecting (25) in the computations may lead to the appearance of so-called spurious modes, and that a possible cure to this problem in the context of a nodal finite element solution is to penalize (25) by including it in the variational formulation derived from Eq. (24) which reads:

Find $\mathbf{E}_1$, such that for all $\mathbf{F}$

$$\begin{aligned} &\int_\Omega (\nabla \times \mathbf{E}_1) \cdot (\nabla \times \bar{\mathbf{F}})\, d\Omega - \int_\Gamma ((\nabla \times \mathbf{E}_1) \times \nu) \cdot \bar{\mathbf{F}}\, d\Gamma \\ &\quad - \int_\Omega (\varepsilon \mathbf{E}_1) \cdot \bar{\mathbf{F}} d\Omega + \int_\Omega \chi \nabla \cdot (\varepsilon \mathbf{E}_1) \overline{\nabla \cdot (\varepsilon \mathbf{F})}\, d\Omega \\ &\quad = -i\omega\mu_0 \int_\Omega \mathbf{J}_{ext,1} \cdot \bar{\mathbf{F}}\, d\Omega + i\omega\mu_0 \int_\Omega \chi \nabla \cdot \mathbf{J}_{ext,1} \overline{\nabla \cdot (\varepsilon \mathbf{F})}\, d\Omega, \end{aligned} \tag{26}$$

where ν is the outgoing unit normal vector with respect to the boundary Γ of the domain Ω.

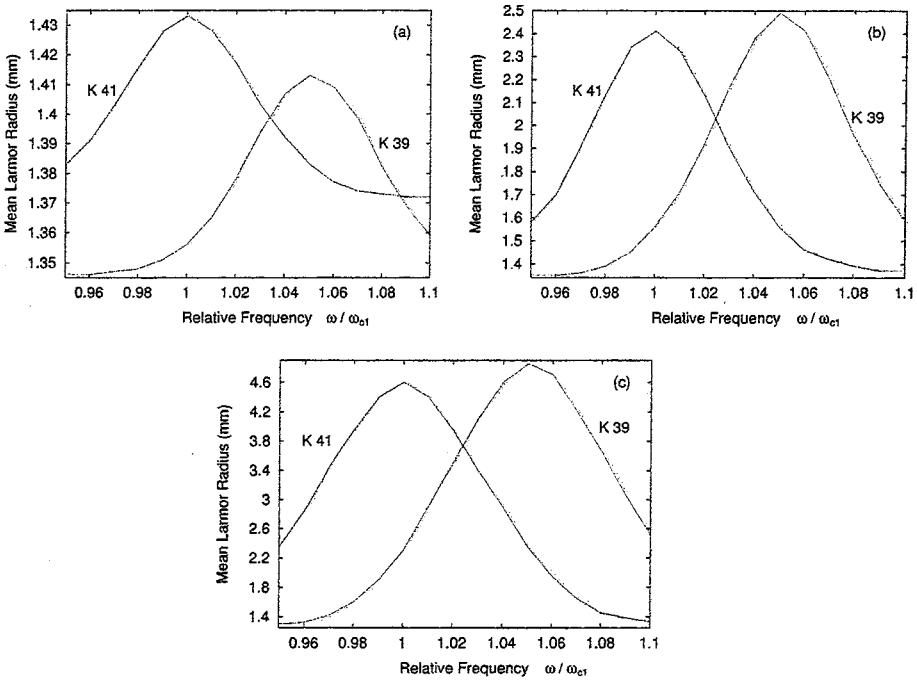

FIG. 4. Mean Larmor radius of the ^{39}K and ^{41}K species in $z = 0.45$ m and in $R = 0$ (a), $R = 2$ cm (b) and $R = 5$ cm (b), as a function of $\frac{\omega}{\omega_{c1}}$.

In the vacuum part of the domain, the penalization parameter χ is chosen to be $\frac{c^4}{\omega^4}$, so that

$$\chi \nabla \cdot (\varepsilon \mathbf{E}_1) \nabla \cdot (\varepsilon \mathbf{F}) = \nabla \cdot \mathbf{E}_1 \nabla \cdot \mathbf{F} \text{ in the vacuum.} \tag{27}$$

For nondiagonal tensors of the form (22), the choice for χ is less obvious. To be coherent with the vacuum case, one can use $\chi = \frac{1}{|\mathrm{Det}(\varepsilon)|^{\frac{2}{3}}}$, where $\mathrm{Det}(\varepsilon)$ is the determinant of ε.

3.2.2. Boundary conditions. The set Γ is composed of the lateral boundary of the cylinder (denoted by Γ_C), on which perfectly conducting conditions ($\mathbf{E}_1 \times \nu = 0$) are imposed, and of its two ends perpendicular to the external magnetic field (commonly denoted by Γ_A). The injection end is a metallic diaphragm, and the terminal end is a metallic collector. Thus, a first option is to simulate the whole device and to apply perfectly conducting conditions on Γ_A. But, in order to lower the computational costs, a second option is to restrict the domain by using artificial vertical boundaries on which absorbing boundary conditions for the wave equation (24) are applied.

For constant scalar permittivity ε and permeability μ, such artificial absorbing boundary conditions are well-known [17]. They read

$$(\nabla \times \mathbf{E}) \times \nu = i \frac{\omega}{\sqrt{\varepsilon \mu}} ((\mathbf{E} \times \nu) \times \nu), \tag{28}$$

and are exact for tangential waves whose propagation vector is normal to the boundary.

Therefore, we look for a condition linking $\mathbf{E}_1$ and $(\nabla \times \mathbf{E}_1) \times \nu$ for plane waves satisfying the homogeneous Eq. (24) and which are tangential and propagating normally to the boundary.

The following relation is obtained (see Ref. [12] for its derivation),

$$(\nabla \times \mathbf{E}_1) \times \nu = i((\sqrt{\varepsilon}_+ \mathbf{E}_1) \times \nu) \times \nu, \tag{29}$$

where the matrix $\sqrt{\varepsilon}_+$ is the square root of ε whose eigenvalues have positive real parts. It reads

$$\sqrt{\varepsilon}_+ = \begin{pmatrix} \left(\frac{k_R + k_L}{2}\right) & -i\left(\frac{k_R - k_L}{2}\right) & 0 \\ i\left(\frac{k_R - k_L}{2}\right) & \left(\frac{k_R + k_L}{2}\right) & 0 \\ 0 & 0 & k_P \end{pmatrix}, \tag{30}$$

where k_R, k_L and k_P are complex numbers such that

$$k_R^2 = \frac{\omega^2}{c^2} - \omega\mu_0(a - b), \ \Re e(k_R) \geq 0, \tag{31}$$

$$k_L^2 = \frac{\omega^2}{c^2} - \omega\mu_0(a + b), \ \Re e(k_L) \geq 0, \tag{32}$$

$$k_P^2 = \frac{\omega^2}{c^2} - \omega\mu_0 r, \ \Re e(k_P) \geq 0, \tag{33}$$

with the definitions

$$a = \frac{n_{e,0}q^2}{m_e} a_e + a^{k+1}, \quad b = \frac{n_{e,0}q^2}{m_e} b_e + b^{k+1}, \quad r = \frac{n_{e,0}q^2}{m_e} r_e + r^{k+1}. \tag{34}$$

For symmetry reasons, and noting that for tangential fields

$$\mathbf{E}_1 = -(\mathbf{E}_1 \times \nu) \times \nu, \tag{35}$$

the insertion of (29) into the variational formulation (26) yields the problem:

Find $\mathbf{E}_1$, with $\mathbf{E}_1 \times \nu_{|\Gamma_C} = 0$ such that for all $\mathbf{F}$ with $\mathbf{F} \times \nu_{|\Gamma_C} = 0$

$$\begin{aligned} &\int_\Omega (\nabla \times \mathbf{E}_1) \cdot (\nabla \times \bar{\mathbf{F}})\, d\Omega + i \int_{\Gamma_A} \sqrt{\varepsilon}_+((\mathbf{E}_1 \times \nu) \times \nu) \cdot ((\bar{\mathbf{F}} \times \nu) \times \nu)\, d\Gamma_A \\ &\quad - \int_\Omega (\varepsilon \mathbf{E}_1) \cdot \bar{\mathbf{F}}\, d\Omega + \int_\Omega \chi \nabla \cdot (\varepsilon \mathbf{E}_1) \overline{\nabla \cdot (\varepsilon \mathbf{F})}\, d\Omega \\ &= -i\omega\mu_0 \int_\Omega \mathbf{J}_{ext,1} \cdot \bar{\mathbf{F}}\, d\Omega + i\omega\mu_0 \int_\Omega \chi \nabla \cdot \mathbf{J}_{ext,1} \overline{\nabla \cdot (\varepsilon \mathrm{F})}\, d\Omega. \end{aligned} \tag{36}$$

3.2.3. Solution of the Discretized Problem. We first define Ω_h as a suitable approximation of the domain Ω, Υ_h as the set of all tetrahedra of a mesh covering Ω_h, and as I_h the set of all vertices of the elements of Υ_h. We denote by Γ_{Ch} (resp. Γ_{Ah}) the boundary of the mesh approximating Γ_C (resp. Γ_A) and by $\Upsilon_h^{\Gamma_{Ch}}$ the set of all triangles which are the traces on Γ_{Ch} of tetrahedra of Υ_h. Finally, $I_h^{\Gamma_{Ch}}$ denotes the set of all vertices of the elements of $\Upsilon_h^{\Gamma_{Ch}}$.

In each node j of $I_h^{\Gamma_{Ch}}$, we define the outward normal vector ν^j in the following way

$$\nu^j = \frac{\sum_{K_h^{\Gamma_{Ch}} \in S(j)} \left|K_h^{\Gamma_{Ch}}\right| \nu_K}{\sum_{K_h^{\Gamma_{Ch}} \in S(j)} \left|K_h^{\Gamma_{Ch}}\right|}, \tag{37}$$

where $|K_h^{\Gamma_{Ch}}|$ designates the area of the triangle $K_h^{\Gamma_{Ch}}$, $S(j)$ the set of all triangles of $\Upsilon_h^{\Gamma_{Ch}}$ to which j belongs, and ν_K is the outgoing normal unit vector of $K_h^{\Gamma_{Ch}}$.

Then we define

$$Y_h = \left\{\mathbf{F}_h \in \mathcal{C}^0(\bar{\Omega}_h)^3; \forall K_h \in \Upsilon_h,\ (\mathbf{F}_h)_{|K_h} \in P_1(K_h)^3\right\}, \tag{38}$$

$$Y_{0h} = \left\{\mathbf{F}_h \in Y_h; \mathbf{F}_h(\mathbf{X}_j) \times \nu^j = 0, \forall j \in I_h^{\Gamma_{Ch}}\right\}, \tag{39}$$

where $\mathbf{X}_j$ are the coordinates of the vertex $j \in I_h^{\Gamma_{Ch}}$. Moreover, we define Π as the orthogonal projection from Y_h onto Y_{0h}. The discrete problem is now:

Find $\mathbf{E}_h \in Y_{0h}$ such that for all $\mathbf{F}_h \in Y_h$,

$$\begin{aligned}
&\int_{\Omega_h} (\nabla \times \Pi\mathbf{E}_h) \cdot (\nabla \times \overline{\Pi\mathbf{F}_h})\, d\Omega_h + i \int_{\Gamma_{Ah}} \sqrt{\varepsilon}_+((\Pi\mathbf{E}_h \times \nu) \times \nu) \cdot ((\overline{\Pi\mathbf{F}_h} \times \nu) \times \nu) d\Gamma_{Ah} \\
&\quad - \int_{\Omega_h} (\varepsilon \Pi\mathbf{E}_h) \cdot \overline{\Pi\mathbf{F}_h}\, d\Omega_h + \int_{\Omega_h} \chi \nabla \cdot (\varepsilon\mathbf{E}_h) \overline{\nabla \cdot (\varepsilon \Pi\mathbf{F}_h)}\, d\Omega_h \\
&= -i\omega\mu_0 \int_{\Omega_h} \mathbf{J}_h \cdot \overline{\Pi\mathbf{F}_h} d\Omega_h + i\omega\mu_0 \int_{\Omega_h} \chi \nabla \cdot \mathbf{J}_h \overline{\nabla \cdot (\varepsilon \Pi\mathbf{F}_h)}\, d\Omega_h,
\end{aligned} \tag{40}$$

where $\mathbf{J}_h$ is a P^1 approximation of $\mathbf{J}_{ext,1}$.

A basis of Y_h can be constructed by associating to each vertex $i \in I_h$ the vectorial function of Y_h

$$\phi_\alpha^i(\mathbf{X}) \in \mathbb{R}^3, \quad \phi_\alpha^i(\mathbf{X}) = \phi^i(\mathbf{X}) e_\alpha, \quad \alpha \in \{x; y; z\}, \tag{41}$$

where we recall that (e_x, e_y, e_z) is the orthonormal basis of $\mathbb{R}^3$, and where $\phi^i(\mathbf{X})$ is the scalar function which is P^1 on each tetrahedron of Υ_h, continuous on $\overline{\Omega_h}$, and such that

$$\forall (i, j) \in I_h^2, \quad \phi^i(\mathbf{X}_j) = \delta^{ij}, \tag{42}$$

where δ^{ij} is the Kronecker symbol.

Equipping Y_h with the scalar product associated to the quadrature formula

$$\int_{\Omega_h} A_h \cdot \overline{B_h}\, d\Omega_h \approx \sum_{K_h \in \Upsilon_h} \frac{|K_h|}{4} \sum_{j \in T(K_h)} A_h(\mathbf{X}_j) \cdot \overline{B_h}(\mathbf{X}_j), \tag{43}$$

where $T(K_h)$ is the set of the four vertices of the tetrahedron K_h, the projection Π has the following expression:

$$\Pi\phi_\alpha^i = \begin{cases} \phi_\alpha^i & \text{if } i \notin I_h^{\Gamma_C}, \\ \sum_{\beta \in \{x;y;z\}} \frac{\nu_\alpha^i \nu_\beta^i}{\|\nu^i\|^2} \phi_\beta^i & \text{if } i \in I_h^{\Gamma_C}\ . \end{cases} \tag{44}$$

Let us write the unknown function as

$$\mathrm{E}_h(\mathbf{X}) = \sum_{\beta\in\{x;y;z\}} \left(\sum_{j\in I_h} E_\beta^j \phi_\beta^j(\mathbf{X}) \right), \quad E_\beta^j \in \mathbb{C}. \tag{45}$$

Suppose further that $\mathbf{J}_h$ is given under the form

$$\mathbf{J}_h(\mathbf{X}) = \sum_{\beta\in\{x;y;z\}} \left(\sum_{j\in I_h} J_\beta^j \phi_\beta^j(\mathbf{X}) \right), J_\beta^j \in \mathbb{C}, \tag{46}$$

and let us denote by $\tilde{\mathbf{E}}$ the vector of $(\mathbb{C}^{Card(I_h)})^3$ of general term $(\tilde{\mathbf{E}})_\beta^j = E_\beta^j$, and by $\tilde{\mathbf{J}}$ the vector of general term $(\tilde{\mathbf{J}})_\beta^j = J_\beta^j$. Then solving problem (40) amounts to finding the solution $\tilde{\mathbf{E}}$ (such that $\tilde{\Pi}\tilde{\mathbf{E}} = \tilde{\mathbf{E}}$) of the following linear system

$$\tilde{\Pi}\tilde{A}\tilde{\Pi}\tilde{\mathbf{E}} = \tilde{\Pi}\tilde{D}\tilde{\mathbf{J}}, \tag{47}$$

where $\tilde{\Pi}$ is the matrix associated to the projection Π, $\tilde{A}$ the matrix whose general term $(\tilde{A})_{\alpha\beta}^{ij}$ is obtained by replacing $\mathbf{E}_h$ by ϕ_β^j and $\mathbf{F}_h$ by ϕ_α^i in the left-hand side of Eq. (40), and $\tilde{D}$ the matrix whose general term $(\tilde{D})_{\alpha\beta}^{ij}$ is obtained by replacing $\mathbf{J}_h$ by ϕ_β^j and $\mathbf{F}_h$ by ϕ_α^i in the right-hand side of Eq. (40).

As we intend to inverse the linear system resulting from the variational formulation in a large domain with fine meshes, it is worth using iterative methods rather than direct ones. The QCGS method [18, 19] has been preferred to other classical methods, such as QMR [20] and conjugate gradient [21], because it ensures the decreasing of the residue at each iteration and can be used with nonhermitian matrices. Like with most iterative methods, it is straightforward to check that applying QCGS to (47) produces at each step an iterate $\tilde{\mathbf{E}}$ which is such that $\tilde{\Pi}\tilde{\mathbf{E}} = \tilde{\mathbf{E}}$, thus addressing correctly the treatment of perfectly conducting boundary conditions.

Test cases reported in [12] have been successfully performed in a cylindrical waveguide filled with two dielectric media and with a solenoidal exciting current density, in order to make a simulation as close as possible to the one we shall finally consider in Section 4. In particular, the necessity of penalizing (25) in the variational formulation was demonstrated, as no convergence of the QCGS method was obtained without penalization.

3.3. *Solution of the Vlasov Equation*

Once the EM field is computed, the next step in the proposed iterative method is to find a $\frac{2\pi}{\omega}$ periodic solution of Eq. (14), subject to the boundary conditions (12) and (13).

3.3.1. A periodic solution. Let us suppose that a particle approximation of the incoming flux on the injection boundary is known under the form

$$-\mathbf{V}\cdot\nu(\mathbf{X})\, f_B(\mathbf{X},\mathbf{V},t) = \left(\sum_{p\in[1,P]} g_p \delta(\mathbf{X}-\mathbf{X}_p)\otimes\delta(\mathbf{V}-\mathbf{V}_p) \right) \otimes \sum_{m\in\mathbb{N}} \delta(t-m\Delta t). \tag{48}$$

This means that at each time step, P particles are introduced in the domain of computation in $(\mathbf{X}_p)_{p\in[1,P]}$ with velocities $(\mathbf{V}_p)_{p\in[1,P]}$. The time step size is chosen to be

$$\Delta t = \frac{2\pi}{\omega N}, \quad \text{with } N \in \mathbb{N}^*. \tag{49}$$

The determination of such an approximation will not be detailed here and can be achieved for example by using a so-called Quiet Start method. We refer to [22] for details on this item.

In order to construct a periodic solution of Eq. (14) subject to the boundary conditions (12) and (13), we consider the corresponding initial value problem (12)–(14) with $f_\alpha(\mathbf{X}, \mathbf{V}, t = 0) = 0$; $\forall(\mathbf{X}, \mathbf{V}) \in \Omega \times \mathbb{R}^3$, and we shall show that its solution is periodic for all times t greater than some value T^* to be given below.

Let us introduce in a classical way the characteristic curves associated to the particle emitted in $\mathbf{X}_p$ with velocity $\mathbf{V}_p$ at time $m\Delta t$

$$\begin{aligned}\left(\mathbf{X}_{\mathbf{X}_p,\mathbf{V}_p,m\Delta t}, \mathbf{V}_{\mathbf{X}_p,\mathbf{V}_p,m\Delta t}\right): \mathbb{R} &\to \Omega \times \mathbb{R}^3 \\ s &\mapsto \left(\mathbf{X}_{\mathbf{X}_p,\mathbf{V}_p,m\Delta t}(s), \mathbf{V}_{\mathbf{X}_p,\mathbf{V}_p,m\Delta t}(s)\right),\end{aligned} \tag{50}$$

which are the solutions of the differential system

$$\begin{aligned}\frac{d\mathbf{X}_{\mathbf{X}_p,\mathbf{V}_p,m\Delta t}(s)}{ds} &= \mathbf{V}_{\mathbf{X}_p,\mathbf{V}_p,m\Delta t}(s) \\ \frac{d\mathbf{V}_{\mathbf{X}_p,\mathbf{V}_p,m\Delta t}(s)}{ds} &= \frac{q}{m}\Big[\mathbf{E}\left(\mathbf{X}_{\mathbf{X}_p,\mathbf{V}_p,m\Delta t}(s), s\right) \\ &\quad + \mathbf{V}_{\mathbf{X}_p,\mathbf{V}_p,m\Delta t}(s) \times \mathbf{B}\left(\mathbf{X}_{\mathbf{X}_p,\mathbf{V}_p,m\Delta t}(s), s\right)\Big] \\ \mathbf{X}_{\mathbf{X}_p,\mathbf{V}_p,m\Delta t}(m\Delta t) &= \mathbf{X}_p \\ \mathbf{V}_{\mathbf{X}_p,\mathbf{V}_p,m\Delta t}(m\Delta t) &= \mathbf{V}_p,\end{aligned} \tag{51}$$

with $\mathbf{E}$ and $\mathbf{B}$ given by

$$\mathbf{E}(\mathbf{X}, t) = \mathbf{E}_1(\mathbf{X})e^{i\omega t} + \overline{\mathbf{E}_1}(\mathbf{X})e^{-i\omega t}, \tag{52}$$

$$\mathbf{B}(\mathbf{X}, t) = \mathbf{B}_0 + \mathbf{B}_1(\mathbf{X})e^{i\omega t} + \overline{\mathbf{B}_1}(\mathbf{X})e^{-i\omega t}, \tag{53}$$

consistently with Eq. (14).

Let us also define the "outgoing time" of a characteristic curve

$$\tau_s(\mathbf{X}_p, \mathbf{V}_p, m\Delta t) = \inf_s \left\{s \geq m\Delta t, \left(\mathbf{X}_{\mathbf{X}_p,\mathbf{V}_p,m\Delta t}(s), \mathbf{V}_{\mathbf{X}_p,\mathbf{V}_p,m\Delta t}(s)\right) \in F_+ \cup F_0\right\} \tag{54}$$

as the moment in which the curve intersects the boundary $F_+ \cup F_0$ defined by

$$F_+ = \{(\mathbf{X}, \mathbf{V}) \in \Gamma \times \mathbb{R}^3,\ \mathbf{V} \cdot \nu(\mathbf{X}) > 0\}, \tag{55}$$

$$F_0 = \{(\mathbf{X}, \mathbf{V}) \in \Gamma \times \mathbb{R}^3,\ \mathbf{V} \cdot \nu(\mathbf{X}) = 0\}, \tag{56}$$

where we recall that Γ is the boundary of the domain, and where $\nu(\mathbf{X})$ is the outgoing normal unit vector of Γ in point $\mathbf{X}$.

The solution of the initial value problem under consideration is given by

$$f(\mathbf{X},\mathbf{V},t) = \sum_{m\in\mathbb{N}} \sum_{p\in[1,P]} g_p \big[H_{m\Delta t}(t) - H_{\tau_s(\mathbf{X}_p,\mathbf{V}_p,m\Delta t}(t)\big] \times \delta\big(\mathbf{X} - \mathbf{X}_{\mathbf{X}_p,\mathbf{V}_p,m\Delta t}(t)\big) \otimes \delta\big(\mathbf{V} - \mathbf{V}_{\mathbf{X}_p,\mathbf{V}_p,m\Delta t}(t)\big), \tag{57}$$

where the Heavyside function $H_u(s)$ is defined by

$$H_u(s) = \begin{cases} 0 & \text{if } s < u \\ 1 & \text{if } s \geq u \end{cases}. \tag{58}$$

Let us now assume that all injected particles reach the "outgoing" boundary within a finite time and let us define

$$\begin{aligned} T^* &= \sup \tau_s(\mathbf{X}_p,\mathbf{V}_p,m\Delta t) \ < +\infty. \\ m &\in [0,N[\\ p &\in [1,P] \end{aligned} \tag{59}$$

Under this hypothesis, the solution (57) of the initial value problem is $\frac{2\pi}{\omega}$ periodic, for times greater than T^*,

$$\forall q \in \mathbb{N}, q \geq \frac{T^*}{\Delta t}, \quad f(\mathbf{X},\mathbf{V},(q+N)\Delta t) = f(\mathbf{X},\mathbf{V},q\Delta t). \tag{60}$$

The proofs of (57) and (60) are not given here (they can be found in [12]), but one can easily understand these properties. Equation (57) states that the delta functions are transported along their characteristic curves.

The weight $[H_{m\Delta t}(t) - H_{\tau_s(\mathbf{X}_p,\mathbf{V}_p,m\Delta t)}(t)]$ is here to ensure that the contribution of the particle injected in $(\mathbf{X}_p,\mathbf{V}_p,m\Delta t)$ is zero before it is injected (for $t < m\Delta t$) and vanishes after it has gone out of the domain (for $t > \tau_s(\mathbf{X}_p,\mathbf{V}_p,m\Delta t)$).

Equation (60) simply states that a particle injected in $(\mathbf{X}_p,\mathbf{V}_p,(m+N)\Delta t)$ follows the same characteristic curve as that injected in $(\mathbf{X}_p,\mathbf{V}_p,m\Delta t)$, and f is thus periodic as soon as all the particles injected during the first N time steps are already out of the domain.

The values of $\mathbf{J}_{i,1}$ and $n_{i,0}$ at the vertices of the tetrahedra are now needed to compute the tensors σ_i and σ_e defined by Eqs. (21) and (23). For the sake of compatibility with the finite element method described in Section 3.2, we use a P^1 approximation of these quantities

$$\mathbf{J}_{i,1}(\mathbf{X}) \approx \sum_{\beta\in\{x,y,z\}} \sum_{j\in I_h} \mathbf{J}^j_{i,1,\beta}\phi^j_\beta(\mathbf{X}), \tag{61}$$

$$n_{i,0}(\mathbf{X}) \approx \sum_{j\in I_h} n^j_{i,0}\phi^j(\mathbf{X}), \tag{62}$$

where ϕ^j and ϕ^j_β are the basis functions defined in Section 3.2.3. Using the quadrature formula (43), we have

$$\int_\Omega \mathbf{J}_{i,1}(\mathbf{X})\phi^j_\beta(\mathbf{X})\,d\Omega \approx M^j\mathbf{J}^j_{i,1,\beta} \quad \text{and} \quad \int_\Omega n_{i,0}(\mathbf{X})\phi^j(\mathbf{X})\,d\Omega \approx M^j n^j_{i,0}, \tag{63}$$

where M^j is defined by

$$M^j = \sum_{K_h \subset Supp(\phi^j)} \frac{|K_h|}{4}. \tag{64}$$

Using formula (57), definitions (17) and (18) and denoting by Q_s the integer part of $\frac{\tau_s(\mathbf{X}_p, \mathbf{V}_p, I\Delta t)}{\Delta t}$, we obtain after some algebra

$$M^j \mathbf{J}^j_{i,1} = \frac{q_i}{N} \sum_{p \in [1,P]} g_p \sum_{I=0}^{N-1} \sum_{k=I}^{Q_s} \mathbf{V}_{\mathbf{X}_p, \mathbf{V}_p, I\Delta t} \left(\left(k + \frac{1}{2} \right) \Delta t \right) \times e^{-i\omega(k+\frac{1}{2})\Delta t} \phi^j \left(\mathbf{X}_{\mathbf{X}_p, \mathbf{V}_p, I\Delta t}((k+1)\Delta t) \right), \tag{65}$$

$$M^j n^j_{i,0} = \frac{q_i}{N} \sum_{p \in [1,P]} g_p \sum_{I=0}^{N-1} \sum_{k=I}^{Q_s} \phi^j \left(\mathbf{X}_{\mathbf{X}_p, \mathbf{V}_p, I\Delta t}((k+1)\Delta t) \right). \tag{66}$$

These formulae have the crucial implication that it is enough to follow the discrete trajectories of the $P \times N$ particles injected during the first period of the EM field. This number of particles does not depend on T^* which can be quite large for long devices. Note that for fixed (p, I, k), the value of $\phi^j(\mathbf{X}_{\mathbf{X}_p, \mathbf{V}_p, I\Delta t}((k+1)\Delta t))$ is nonzero only for four vertices j, namely the summits of the tetrahedron in which the particle injected in $(\mathbf{X}_p, \mathbf{V}_p, I\Delta t)$ is present at time $(k+1)\Delta t$. The determination of such a tetrahedron and the computation of $\phi^j(\mathbf{X}_{\mathbf{X}_p, \mathbf{V}_p, I\Delta t}((k+1)\Delta t))$ are performed using the particle tracking method presented in [23]. In the context of ICR heating, the determination of the particle trajectories must be a subject of special care and is described in the next subsection.

3.3.2. Particle pushing. The periodic Larmor motion of the ions around their guiding centers needs to be described accurately because the heating mechanism of a species α is based on the resonance between ω and $\omega_{c\alpha}$. The usual particle pusher of Boris, as described in [22], discretizes the circular uniform motion by a polygon whose perimeter is shorter than that of the circle it approximates, resulting in a slight modification of the effective cyclotron frequency of the particles. As this modification is roughly of the order of the isotope shift between the different isotopic species for usual discretizations (around 1.3% for a polygon with 16 sides), it is absolutely necessary to use a well-adapted particle pusher.

The general idea is the following: Knowing at time $t^{n-\frac{1}{2}}$, the velocity $\mathbf{V}^{n-\frac{1}{2}}$ and at time t^n the position $\mathbf{X}^n$ of an ion and the values of the EM field in $\mathbf{X}^n$, we shall integrate the equation

$$\frac{d\mathbf{V}}{dt} = \frac{q}{m}(\mathbf{E}(\mathbf{X}^n, t) + \mathbf{V}(t) \times \mathbf{B}(\mathbf{X}^n, t)), \quad \mathbf{V}\left(t^{n-\frac{1}{2}}\right) = \mathbf{V}^{n-\frac{1}{2}}, \tag{67}$$

as exactly as possible on the interval $[t^{n-\frac{1}{2}}, t^{n+\frac{1}{2}}]$. In this formula, $\mathbf{E}$ and $\mathbf{B}$ are given by (52) and (53).

After computing the approximation $\mathbf{V}^{n+\frac{1}{2}}$ of the velocity at time $t^{n+\frac{1}{2}}$ the position is updated through the classical scheme

$$\mathbf{X}^{n+1} = \mathbf{X}^n + \Delta t \mathbf{V}^{n+\frac{1}{2}}. \tag{68}$$

Keeping in mind that the combined effects of $\mathbf{E}_1$ and $\mathbf{B}_0$ are the very basis of the cyclotron heating mechanism, we choose to decouple their action of that of $\mathbf{B}_1$ which is orders of magnitude weaker than $\mathbf{B}_0$. We thus take into account the following:

1. Half a rotation resulting from $\mathbf{B}_1$

$$\frac{d\mathbf{V}^{(1)}}{dt} = \frac{q}{m}\left[\mathbf{V}^{(1)} \times (\mathbf{B}_1(\mathbf{X}^n)e^{i\omega n\Delta t} + \overline{\mathbf{B}_1}(\mathbf{X}^n)e^{-i\omega n\Delta t})\right] \quad \text{with} \quad \mathbf{V}^{(1)}(0) = \mathbf{V}^{n-\frac{1}{2}}, \tag{69}$$

2. Then, the effect resulting from $\mathbf{E}_1$ and $\mathbf{B}_0$

$$\frac{d\mathbf{V}^{(2)}}{dt} = \frac{q}{m}\left[\mathbf{E}_1(\mathbf{X}^n)e^{i\omega t} + \overline{\mathbf{E}_1}(\mathbf{X}^n)e^{-i\omega t} + \mathbf{V}^{(2)}(t) \times \mathbf{B}_0\right] \quad \text{with} \quad \mathbf{V}^{(2)}\left(t^{n-\frac{1}{2}}\right) = \mathbf{V}^{(1)}\left(\frac{\Delta t}{2}\right), \tag{70}$$

3. The second half-rotation resulting from $\mathbf{B}_1$

$$\frac{d\mathbf{V}^{(3)}}{dt} = \frac{q}{m}\left[\mathbf{V}^{(3)} \times (\mathbf{B}_1(\mathbf{X}^n)e^{i\omega n\Delta t} + \overline{\mathbf{B}_1}(\mathbf{X}^n)e^{-i\omega n\Delta t})\right] \quad \text{with} \quad \mathbf{V}^{(3)}(0) = \mathbf{V}^{(2)}\left(t^{n+\frac{1}{2}}\right), \tag{71}$$

The final approximation will be computed as

$$\mathbf{V}^{n+\frac{1}{2}} = \mathbf{V}^{(3)}\left(\frac{\Delta t}{2}\right). \tag{72}$$

The steps (69) and (71) do not need a special treatment. Thus, we use the classical Boris pusher whose precision is second order in time, according to the formula

$$\frac{\mathbf{V}^{(j)}\left(\frac{\Delta t}{2}\right) - \mathbf{V}^{(j)}(0)}{\frac{\Delta t}{2}} = \frac{q}{m}\frac{\left(\mathbf{V}^{(j)}\left(\frac{\Delta t}{2}\right) + \mathbf{V}^{(j)}(0)\right)}{2} \times (\mathbf{B}_1(\mathbf{X}^n)e^{i\omega n\Delta t} + \overline{\mathbf{B}_1}(\mathbf{X}^n)e^{-i\omega n\Delta t}), \tag{73}$$

for $j = 1$ or 3.

Practical details to implement this pusher can be found in [22]. On the other hand, Eq. (70) is solved in an exact way. It is first useful to split $\mathbf{V}^{(2)} = (u^{(2)}, v^{(2)}, w^{(2)})$ and $\mathbf{E}_1$ in their parallel and perpendicular components relatively to the magnetic field, i.e., to the vector e_z.

The equation for $w^{(2)}$ is now,

$$\frac{dw^{(2)}}{dt} = \frac{q}{m}[\mathbf{E}_{1z}(\mathbf{X}^n)e^{i\omega t} + \overline{\mathbf{E}_{1z}}(\mathbf{X}^n)e^{-i\omega t}], \tag{74}$$

whose solution is given by

$$w^{(2)}\left(t^{n+\frac{1}{2}}\right) = w^{(2)}\left(t^{n-\frac{1}{2}}\right) + \frac{2q}{\omega m}\sin\left(\frac{\omega\Delta t}{2}\right)[\mathbf{E}_{1z}(\mathbf{X}^n)e^{i\omega n\Delta t} + \overline{\mathbf{E}_{1z}}(\mathbf{X}^n)e^{-i\omega n\Delta t}]. \tag{75}$$

By setting,

$$\mathbf{V}_\perp = u^{(2)} + i v^{(2)}, \tag{76}$$

and

$$\mathbf{E}_\perp^n = \mathbf{E}_{1x}(\mathbf{X}^n) + i\mathbf{E}_{1y}(\mathbf{X}^n), \quad \tilde{\mathbf{E}}_\perp^n = \overline{\mathbf{E}_{1x}}(\mathbf{X}^n) + i\overline{\mathbf{E}_{1y}}(\mathbf{X}^n), \tag{77}$$

we obtain the following equation for $\mathbf{V}_\perp$

$$\frac{d\mathbf{V}_\perp}{dt} = -i\omega_c \mathbf{V}_\perp + \frac{q}{m}\left(\mathbf{E}_\perp^n e^{i\omega t} + \tilde{\mathbf{E}}_\perp^n e^{-i\omega t}\right). \tag{78}$$

As usual, when studying particle motion in the context of ICR, it is necessary to consider two cases

1. Nonresonant cases ($\omega^2 \neq \omega_c^2$), for which there holds

$$\mathbf{V}_\perp^{n+\frac{1}{2}} = \mathbf{V}_\perp^{n-\frac{1}{2}} e^{-i\omega_c \Delta t} + \frac{q}{m}\left[\mathbf{E}_\perp^n e^{i\omega\left(n+\frac{1}{2}\right)\Delta t}\frac{\left(1-e^{-i(\omega_c+\omega)\Delta t}\right)}{i(\omega_c+\omega)} + \tilde{\mathbf{E}}_\perp^n e^{-i\omega\left(n+\frac{1}{2}\right)\Delta t}\frac{\left(1-e^{-i(\omega_c-\omega)\Delta t}\right)}{i(\omega_c-\omega)}\right]. \tag{79}$$

2. We then only consider the resonant case $\omega = \omega_c$, as the other possibility $\omega = -\omega_c$ can be treated in a similar way. The exact solution of (78) is given by

$$\mathbf{V}_\perp^{n+\frac{1}{2}} = \mathbf{V}_\perp^{n-\frac{1}{2}} e^{-i\omega_c \Delta t} + \frac{q}{m}\left[\mathbf{E}_\perp^n e^{i\omega\left(n+\frac{1}{2}\right)\Delta t}\frac{\left(1-e^{-i(\omega_c+\omega)\Delta t}\right)}{i(\omega_c+\omega)} + \tilde{\mathbf{E}}_\perp^n e^{-i\omega\left(n+\frac{1}{2}\right)\Delta t}\Delta t\right]. \tag{80}$$

4. RESULTS

The aim of this section is twofold. First, we test on a rather simple case the convergence of the iterative method proposed to solve the global coupled problem as described in Section 3.1. Second, we check qualitatively that the numerical results meet expected physical characteristics. Detailed analysis of the physics as well as comparisons with experiments are not the matter of this paper and will be reported elsewhere.

4.1. *Simulation Parameters*

We are interested in the simulation of a Potassium plasma composed of two isotopic species: ^{41}K, further denoted as "species 1" and ^{39}K, further denoted as "species 2." All relevant physical parameters will be subscripted either by $_1$ or by $_2$ whether they refer to species 1 or 2, respectively.

The computational domain is a cylinder of length 50 cm and of radius 15 cm, which represents the heating region of a fictitious separation device. For information, the length of actual devices, as described for example in [3] and [24] may vary from 0.5 m to 2 m.

On the injection section of this cylinder (located in $z = 0$) the distribution functions of the two ion species are given by

$$f_{\alpha,B}(x, y, u, v, w) = \begin{cases} \left(1 - \frac{R^2}{R_p^2}\right)^p n_0 a_\alpha \tilde{g}_{\alpha,B}(v_\perp, v_\parallel) & \text{if } R \leq R_p \\ 0 & \text{if } R \geq R_p, \end{cases} \tag{81}$$

where we set

$$R^2 = x^2 + y^2, \quad v_\perp^2 = u^2 + v^2, \quad v_\parallel = w. \tag{82}$$

The function $\tilde{g}_{\alpha,B}$ is supposed to be Maxwellian

$$\tilde{g}_{\alpha,B}(v_\perp, v_\parallel) = \frac{1}{\pi^{\frac{3}{2}} V_{Th,\alpha}^3} e^{-\frac{(v_\parallel - \bar{w}_\alpha)^2}{V_{Th,\alpha}^2} - \frac{v_\perp^2}{V_{Th,\alpha}^2}}, \tag{83}$$

and n_0 designates the total ion density at the center of the plasma column, p is a real number determined by the experimental conditions, R_p is the radius of the plasma column at the entrance of the heating zone, a_α represents the proportion of species α in the plasma, $\bar{w}_\alpha$ is the mean axial velocity, and $V_{Th,\alpha}$ the thermal velocity computed from the temperature T_α by the following formula

$$V_{Th,\alpha} = \sqrt{\frac{2KT_\alpha}{m_\alpha}}. \tag{84}$$

For the simulation presented here, we choose the following parameters

$$n_0 = 5.10^{16}\,\text{particles.m}^{-3}, \quad p = 1.5, \quad R_p = 6\ \text{cm}, \tag{85}$$

$$a_1 = 0.069, \quad a_2 = 0.931, \quad T_1 = T_2 = 0.2\text{eV}, \quad \bar{w}_1 = \bar{w}_2 = 3000\ \text{m.s}^{-1}. \tag{86}$$

The magnetic field strength $|\mathbf{B}_0|$ is chosen to be 0.3 T. The antenna which carries the electric current is a simple solenoidal sheet

$$\mathbf{J}_{ext,1}(R, \theta, z) = \begin{pmatrix} 0 \\ J_\theta \\ 0 \end{pmatrix} \delta(R - R_a) \mathbb{1}_{z \in [z_m; z_M]}, \tag{87}$$

where δ is the Dirac distribution located in $R = R_a = 8.5$ cm. Moreover, the antenna extends axially from $z_m = 0.1$ m to $z_M = 0.4$ m and carries a current $J_\theta = 900\ \text{A.m}^{-1}$.

Under these conditions, the value of the ion–ion collision frequency at the center ($R = 0$) of the plasma column and at the entrance of the heating zone is found to be around $6.10^4\ \text{s}^{-1}$. Note that this value decreases both radially, because of the density profile as given by Eq. (81), and axially, in a strong way, as heating raises the temperature species (see Figs. 5 and 6). Thus, the simulation presented here reaches the limit of applicability of the noncollisional assumption for those particles which are at the center of the column: with the mean axial velocity indicated above, such particles will, in the mean, experience a few collisions during their transit in the heating zone. However, this may hardly affect the results presented here because the accelerating electric field is anyway zero on the axis, as can be seen from Fig. 7. Inclusion of an ion–ion collision operator would be required to study the effect of the noncollisional hypothesis on the numerical results, but is out of the scope of this article.

The computational domain is covered by two meshes (a coarse one and a finer one). They are further denoted by M_1 (respectively M_2) and are composed of 5607 (resp. 38581) nodes and 30240 (resp. 218880) tetrahedra. The axial length of 0.5 m is discretized by

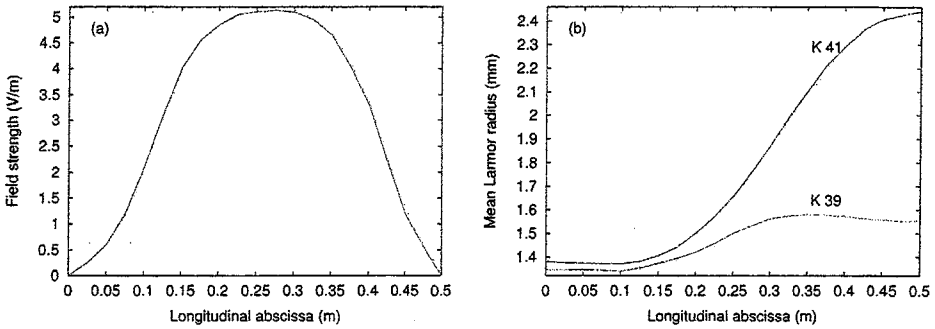

FIG. 5. Longitudinal profile of the field $|\tilde{\mathbf{E}}_\perp|$ (a) and of the mean Larmor radius of isotopes ^{39}K and ^{41}K (b) in $R = 2$ cm for $\omega = \omega_{c1}$.

21 (resp. 41) nodes and there are 267 (resp. 941) nodes in a section of the mesh. Moreover, the wave period is divided into 16 (resp. 32) time steps for simulations on M_1 (resp. M_2) and 1664 (resp. 13312) particles of each of the two species are injected at each time step, which corresponds to 8 (resp. 16) particles per triangle belonging to the trace of the mesh on the injection section of the cylinder.

4.2. *Numerical Results*

In order to evaluate the convergence of the iterative method proposed in Section 3.1, we define two criteria D^k and Dp^k which measure the relative difference between the electric fields obtained at iterations k and $k-1$ in the whole domain and in the part of the domain filled with plasma, respectively. More precisely; we define

$$\mathrm{Dp}^k = \sqrt{\frac{\sum_{j \in I_h^P} M^j \left\| \left(\mathrm{E}_h^j\right)^k - \left(\mathrm{E}_h^j\right)^{k-1} \right\|^2}{\sum_{j \in I_h^P} M^j \left\| \left(\mathrm{E}_h^j\right)^k \right\|^2}}, \tag{88}$$

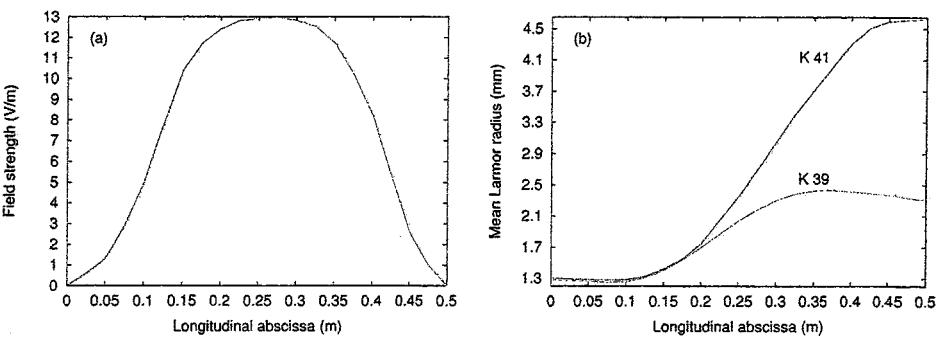

FIG. 6. Longitudinal profile of the field $|\tilde{\mathbf{E}}_\perp|$ (a) and of the mean Larmor radius of isotopes ^{39}K and ^{41}K (b) in $R = 5$ cm for $\omega = \omega_{c1}$.

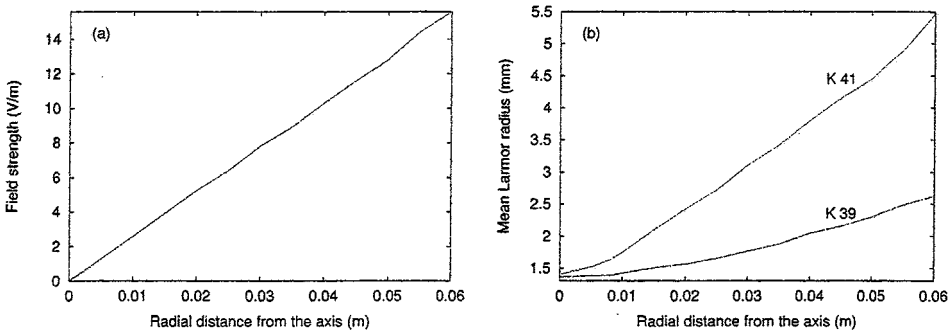

FIG. 7. Radial profile of the field $|\tilde{\mathbf{E}}_\perp|$ in $z = 0.25$ m (a) and of the mean Larmor radius of isotopes ^{39}K and ^{41}K (b) in $z = 0.45$ m for $\omega = \omega_{c1}$.

and

$$\mathrm{D}^k = \sqrt{\frac{\sum_{j\in I_h} M^j \left\| \left(\mathrm{E}_h^j\right)^k - \left(\mathrm{E}_h^j\right)^{k-1} \right\|^2}{\sum_{j\in I_h} M^j \left\| \left(\mathrm{E}_h^j\right)^k \right\|^2}}, \tag{89}$$

where $(\mathrm{E}_h^j)^k$ is the value of the field E_h at node j and at iteration k, and where I_h^P is the subset of I_h composed of the nodes that are located in the plasma region ($R \le R_P$).

The quantities Dp^k and D^k are presented on Figs. 2 and 3 for $\omega = 0.95\ \omega_{c1}$ and $\omega = \omega_{c1}$, respectively, and for simulations performed on mesh M_1. Fast convergence is observed with $\omega = 0.95\omega_{c1}$, when the cyclotron heating is rather low. On the other hand, the first iteration for $\omega = \omega_{c1}$, when the heating of species 1 is maximum, computes only a crude approximation of the converged value of the electric field and a supplementary iteration seems to be necessary to reach the same criteria as in the $\omega = 0.95\omega_{c1}$ case.

Further, we give in Table I the CPU time needed to compute a solution of the Maxwell equations ("M step") and of the two ion Vlasov equations ("V step") on both meshes on a CRAY T3D vector computer. Obviously, computations on the coarser mesh are rather cheap and enable parametric studies of the separation process by varying parameters, such as wave frequency, confining magnetic field strength, plasma density. We also note that further efforts (e.g., parallelization) should be made to lower the CPU time needed by particle treatment, as this is the most expensive part of the computation. When well-defined parameters have been chosen after a parametric study on the coarser mesh, a more detailed computation can be made within some hours of CPU time on the finer mesh.

TABLE I
CPU Time Needed for the Two Steps of the Iterative Method on Mesh M_1 and M_2

Mesh	Step M	Step V
M_1	2.75 s	105 s
M_2	29.2 s	3718 s

4.3. *Analysis of the Results*

Simulations were performed on M_1 for $\omega \in [0.95\omega_{c1}, 1.10\omega_{c1}]$ with increments of $0.01\omega_{c1}$ in ω. In order to evaluate the efficiency of the selective heating, the mean Larmor radius of the two ion species in the section of the cylinder located in $z = 0.45$ m and for $R = 0$, $R = 2$ cm and $R = 5$ cm was computed as a function of the frequency of the exciting current density. Figure 4 shows that the most efficient pulsation for the heating of species 1 (resp. species 2) is $\omega = \omega_{c1}$ (resp. $\omega = \omega_{c2}$): This indicates the absence of Doppler shift for this type of antenna, a fact which was pointed out in [2].

The longitudinal profiles of the resonant transversal electric field $\tilde{\mathbf{E}}_\perp$, defined by formula (77) and of the mean Larmor radius of species 1 and 2 are presented on Fig. 5 for $R = 2$ cm and 6 for $R = 5$ cm. Recalling that the exciting antenna is located between $z = 10$ cm and $z = 40$ cm, we observe a good transversal homogeneity of the electric field in the region 15 cm $\leq z \leq$ 35 cm, and the mean Larmor radius of the resonant species grows rather linearly in this region. On the other hand, after an initial growth, the mean Larmor radius of the nonresonant species starts to decrease at the end of the column. But as the field is lower in that region, this decrease is weak. In order to get a better selectivity of the method, the heating region should be chosen long enough so that the nonresonant species has lost a maximum of energy at the end of the column.

Finally, Fig. 7 shows that the radial profile of $\tilde{\mathbf{E}}_\perp$ in the section $z = 25$ cm is linear with respect to the radial position. This fact was observed with that type of antenna in [2]. Moreover, as a consequence, the mean Larmor radius of the ions species also varies rather linearly.

5. SUMMARY AND CONCLUSIONS

In this paper, a self-consistent nonlinear model for the ICR isotope separation process was presented for the first time. While the interaction between the electromagnetic field and the ion species is described by the coupling of the time harmonic Maxwell equations and quasilinear Vlasov equations, electrons are assumed to be cold. Further, we introduced a fixed-point iterative method to self-consistently solve this nonlinear set of equations. The Maxwell equations are solved by a finite element method, and the ion Vlasov equations are solved by a particle method specially adapted to the ICR phenomenon. The analysis of a simulation in a simple configuration indicates that this iterative method shows fast convergence and that parametric studies of an actual separation device are reachable for reasonable memory and CPU time costs. Moreover, the presented numerical results meet expected physical features, which justifies our confidence in this method.

REFERENCES

1. T. H. Stix, Fast wave heating of a two-component plasma, *Nucl. Fusion* **15**, 737 (1975).
2. J. M. Dawson, H. C. Kim, D. Arnush, B. D. Fried, R. W. Gould, L. O. Heflinger, C. F. Kennel, T. E. Romesser, R. L. Stenzel, A. Y. Wong, and R. F. Wuerker, Isotope separation in plasmas by use of ion cyclotron resonance, *Phys. Rev. Lett.* **37**, 1547 (1976).
3. A. Compant La Fontaine and P. Louvet, Recent development in stable isotope separation by ionic cyclotron resonance, in *Proceedings of the 2nd. Workshop on Separation Phenomena in Liquids and Gases, Versailles, France, 1989* (CEA Editions, 1989) Vol. 1, p. 139.

4. National Technical Information Center Service, *ICRF Antenna Coupling Theory for a Stratified Plasma*, in Document No. DE85004960, edited by B. D. McVey, Report PFC RR-84-13 (Plasma Fusion Center, MIT, 1984.) Copies may be ordered from the National Technical Information Center, Springfield, VA 22161.
5. A. Compant La Fontaine and V. G. Pashkovsky, Study of selective heating at ion cyclotron resonance for the plasma separation process, *Phys. Plasmas* **2**, 4641 (1995).
6. V. L. Ginzburg and A. A. Ruhadze, in *Handbuch der Physik*, edited by K. Rawer (Springer, Berlin, 1972), Vol. 49/4, p. 395.
7. R. W. Short and A. Simon, Landau damping and transit-time damping of localized plasma waves in general geometries, *Phys. Plasmas* **5**, 4124 (1998).
8. R. V. Jensen and I. B. Bernstein, Ion acoustic waves in finite geometry, *Phys. Fluids* **26**, 953 (1983).
9. A. Compant La Fontaine, P. Louvet, P. Le Gourrierec, and A. Pailloux, Selective heating of high-pressure vapour elements by ion cyclotron resonance, *J. Phys. D: Appl. Phys.* **31**, 847 (1998).
10. T. H. Stix, *Waves in Plasmas* (American Institute of Physics, New York, 1992).
11. M. Bostan and F. Poupaud, Periodic solutions of the Vlasov–Poisson system with boundary conditions, *C.R.A.S Paris (I)* **325**, 1333 (1997).
12. P. Omnes, Résolution numérique des équations de Maxwell-Vlasov en régime périodique. Application à l'étude de la séparation isotopique par résonance cyclotron ionique. Ph.D. thesis (University of Toulouse III, France, 1999).
13. D. Van Eester, Plasma heating and current drive: Numerical methods, *Trans. Fusion Technol.* **25**, 209 (1994).
14. J.-C. Nédélec, Mixed finite elements in $\mathbb{R}^3$, *Numer. Math.* **35**, 315 (1980).
15. G. Mur, Edge elements, their advantages and their disadvantages, *IEEE Trans. Magn.* **30**, 3552 (1994).
16. B. N. Jiang, J. Wu, and L. A. Povinelli, The origin of spurious solutions in computational electromagnetics, *J. Comput. Phys.* **125**, 104 (1996).
17. A. F. Peterson, Absorbing boundary conditions for the vector wave equation, *Microwave Optical Technol. Lett.* **1**, 62 (1988).
18. C. H. Tong, *A comparative Study of Preconditioned Lanczos Methods for Nonsymmetric Linear Systems*, Technical Report SAND91-8240 UC-404 (Sandia National Laboratories Albuquerque, 1992).
19. R. Weiss, Convergence Behavior of Generalized Conjugate Gradient Methods, Ph.D. thesis (University of Karlsruhe, Germany, 1990).
20. R. W. Freund and N. M. Nachtigal, QMR: a quasi-minimal residual method for non-Hermitian linear systems, *Numer. Math.* **60**, 315 (1991).
21. M. R. Hestenes and E. Stiefel, Methods of conjugate gradients for solving linear systems, *J. Res. Natl Bur. Stand.* **49**, 409 (1952).
22. C. K. Birdsall and A. B. Langdon, Plasma Physics via Computer Simulation (McGraw-Hill, New York, 1985).
23. F. Assous, P. Degond, and J. Segré, A particle-tracking method for 3d electromagnetic PIC codes on unstructured meshes, *Comput. Phys. Commun.* **72**, 105 (1992).
24. A. I. Karchevskii, V. S. Laz'ko, Y. A. Muromkin, A. I. Myachikov, V. G. Pashkovsky, A. L. Ustinov, and A. V. Chepkasov, Investigation of Lithium isotope resonant separation in a plasma with isotopically selective ICR heating, *Plasma Phys. Rep.* **19**, 214 (1993).